

Maneuvering simulations of pusher–barge systems

Koh Kho King · Hironori Yasukawa · Noritaka Hirata
Kuniji Kose

Received: January 15, 2007 / Accepted: December 2, 2007
© JASNAOE 2008

Abstract Pusher–barge systems were studied in nine different configurations. Captive model tests were performed at the Hiroshima University Towing Tank and the hydrodynamic derivatives for the various configurations were obtained. At a service speed of 7 knots, pusher–barge systems with the same number of barges but arranged in a row (shorter length overall but with a larger breadth) require more power to operate than those that were arranged in a line. When the length overall increased, the tactical diameter, advance, and transfer distances also increased, mainly due to the significant increase in the moment of inertia when barges are arranged in a line, rather than in a row. All pusher–barge systems had small first and second overshoot angles. Pusher–barge systems with the same number of barges had a longer response time to the rudder angle of attack and required a longer stopping distance when arranged in a line, mainly due to the increased moment of inertia and reduced resistance when barges are arranged in this way.

Key words Pusher–barge · Captive model test · Maneuvering simulations · Hydrodynamic derivatives

1 Introduction

Barges are frequently used in inland waterways for their shallow draft and their ability to transit into the inland waterways network.¹ The common practice of pushing two or more barges with a pusher is widely used in

Europe and America, especially in the Mississippi, Elbe, and Danube rivers. River transportation is more economic for transporting a large quantity of cargo compared to truck or railway transportation because of the high capital investment and maintenance costs required for land transportation. With the ever increasing price of fuel nowadays, there are even more reasons to choose river transportation. Long, wide rivers suitable for barge transportation exist in Southeast Asia, and the use of pusher–barge systems for transporting large amount of goods is worth examining.

With increases in cargo quantity and size, rivers have become more crowded than before.² Accidents tend to happen more frequently due to poor maneuverability and narrow or shallow waterways. The safety of pusher–barge systems with regard to maneuverability needs to be examined, especially for the more complicated cases of multiple barges pushed by one pusher used nowadays. From the economic point of view, more barges being used at one time for transporting large quantity of goods is often more efficient, but with river depth and width changing rapidly and differing from place to place, operational safety should be taken into consideration when deciding the quantity of goods and the number of barges to be used.

A study of the hydrodynamic force characteristics of three barges was conducted in the past,³ but the behavior of four barges or more still remains to be explored. This article examines the maneuverability of nine different configurations of pusher–barge system. In order to examine the operational safety of a pusher–barge system, a study of the control performance is necessary. Models of the pusher and barges were made for this purpose and were tested at the Hiroshima University towing tank to study the motion characteristics of the various configu-

K.K. King (✉) · H. Yasukawa · N. Hirata · K. Kose
Graduate School of Engineering, Hiroshima University,
1-4-1 Kagamiyama, Higashi Hiroshima 739-8527, Japan
e-mail: khoking@gmail.com

rations of pusher–barge system. Maneuvering simulations of the pusher–barge systems were carried out using a program written by the authors in FORTRAN employing suitable motion equations and hydrodynamic derivatives obtained from the model test data. Computer simulations are much cheaper than tank tests and can flexibly adapt to various conditions. In the simulations, the pusher–barge system is considered as one solid body, and hence the computer calculation results and methods can be further developed for other types of vessel in the future.

2 Pusher and barge particulars

A pusher with twin screws and twin rudders was used in this study. The pusher had controllable pitch propellers

with a diameter (D_p) of 1.8 m and a speed of 300 rpm; the main engine power was 1000 kW. The rudders used on the pusher had a span of 2.0 m, a cord of 2.0 m, and area of 4.0 m² each. Figure 1 shows the body plan of the pusher and Table 1 shows the principal dimensions of the pusher at full scale and model scale (scale 1/50). Selection of the pusher, rudders, and propellers was made with reference to Pfennigstorf’s article.⁴

Two types of barges were used in the experiments: the rake barge and the box barge. Table 1 shows the principal particulars of the two barge types and the body plan of the rake barge is shown in Fig. 2. The leading barge was always a rake barge and those between the rake barge and the pusher were always box barges. Only one pusher situated aft of the barge system was used.

Nine different configurations of pusher–barge system were considered in this article. To differentiate the

Fig. 1. Body plan of a pusher. WL, water line; BL, buttock line; FP, forward perpendicular; AP, aft perpendicular

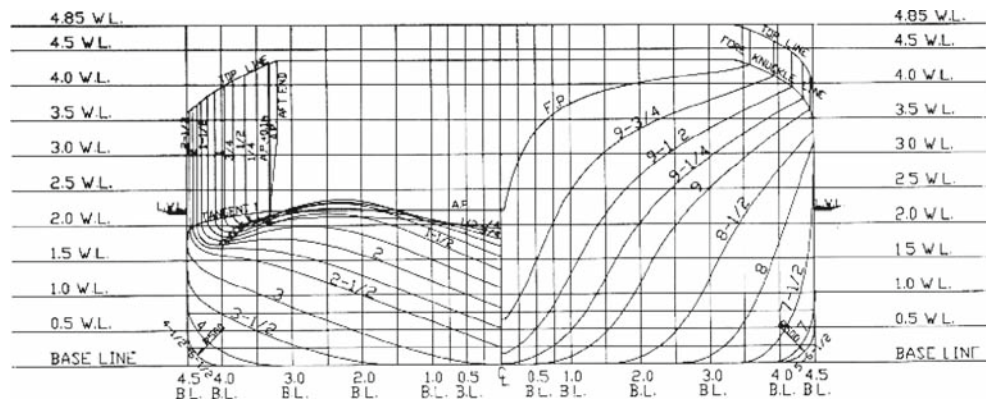


Fig. 2. Body plan of a rake barge. WL, water line; BL, buttock line; FP, forward perpendicular; AP, aft perpendicular

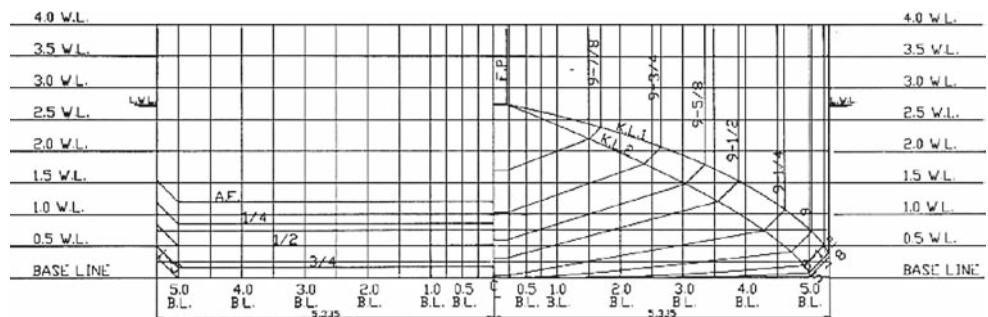


Table 1. Principal full-scale and model dimensions of the pusher, rake barge, and box barge

	Pusher		Box barge		Rake barge	
	Full-scale	Model	Full-scale	Model	Full-scale	Model
Length overall, LOA (m)	40.0	0.80	60.96	1.219	60.96	1.219
Length between perpendiculars, LBP (m)	39.5	0.79	60.96	1.219	60.96	1.219
Breadth, B (m)	9.0	0.18	10.67	0.213	10.67	0.213
Draft, d (m)	2.2	0.044	2.74	0.0548	2.74	0.0548
Volume, ∇ (m ³)	494.7	0.00396	1707.6	0.01366	1646.2	0.0132
Longitudinal center of buoyancy (LCB) from aft perpendicular (AP) (m)	21.98	0.4395	30.48	0.6096	29.44	0.5888
Block coefficient, C_B	0.633	0.633	0.958	0.958	0.924	0.924

Table 2. Principal dimensions of full-scale pusher–barge systems

	11BP	12BP	13BP	21BP	22BP	23BP	31BP	32BP	33BP
LOA (m)	100.96	161.92	222.88	100.96	161.92	222.88	100.96	161.92	222.88
B (m)	10.67	10.67	10.67	21.34	21.34	21.34	32.01	32.01	32.01
d (m)	2.74	2.74	2.74	2.74	2.74	2.74	2.74	2.74	2.74
∇ (m ³)	2140.9	3848.5	5556.1	3787.1	7202.3	10618	5433.3	10556	15679
LCB from AP (m)	58.47	89.88	120.7	63.24	94.54	125.3	65.12	96.24	126.9
C_B	0.725	0.813	0.853	0.642	0.761	0.815	0.614	0.743	0.802

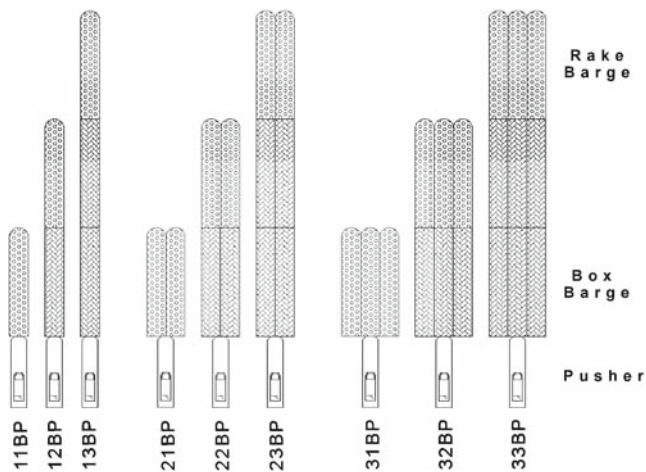


Fig. 3. Pusher–barge system naming designations

various pusher–barge configurations, a naming system of the form “ $ijBP$ ” was used, where i is number of columns and j is the number of rows in the barge system. Figure 3 shows the arrangements of the pusher–barge systems with their designations. Table 2 shows the principal dimensions of the pusher–barge systems at full scale.

3 Simulation method for maneuvering motions

Figure 4 shows the coordinate systems used in the article. $O-X_0Y_0Z_0$ is the space coordinate system, with the X_0Y_0 plane referring to the water surface and Z_0 being vertically downward from the water surface. ψ is the angle between the X_0 axis and the pusher–barge system’s heading. $G-xyz$ is the pusher–barge system’s coordinate system, where G is the center of gravity of the pusher–barge system, x is the forward direction of the pusher–barge system, and y is the lateral direction of the pusher–barge system. The xy plane forms the water surface where the pusher–barge system is located, and z is the vertical downward direction from the center of gravity of the pusher–barge system. The maneuvering motions of the pusher–barge system (surge, sway, and yaw) are defined in the following motion equations:

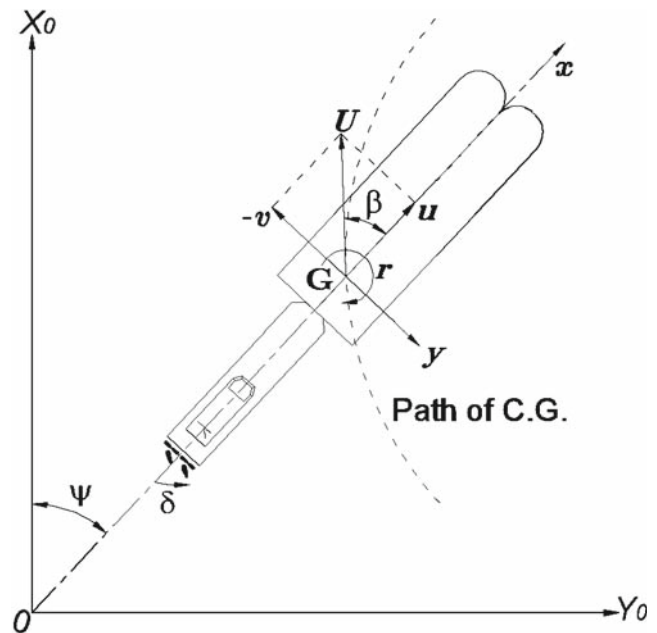


Fig. 4. Coordinate systems. $C.G.$, center of gravity

$$\left. \begin{aligned} (m + m_x)\dot{u} - (m + m_y)vr &= X \\ (m + m_x)ur + (m + m_y)\dot{v} &= Y \\ (I_G + J_{zz})\dot{r} &= N \end{aligned} \right\} \quad (1)$$

where u is the forward speed, v is the lateral speed, r is the yaw rate, m is the mass of the pusher–barge system, and I_G is the moment of inertia of the pusher–barge system. m_x , m_y , and J_{zz} are the added masses and added moment of inertia of the pusher–barge system. On the right hand sides of the equations, X is the total forward force, Y is the total lateral force, and N is the total moment at the center of gravity of the pusher–barge system. X , Y , and N are the forces and moment made up of contributions from the hull (H), propeller (P), and rudder (R), as expressed in Eq. 2. x_G is the longitudinal position from the midship position (at exactly half of the total length of the pusher and barge combination) to the center of gravity with forward direction having a positive value.

$$\left. \begin{aligned} X &= X_H + X_P + X_R \\ Y &= Y_H + Y_R \\ N &= N_H + N_R - (Y_H + Y_R)x_G \end{aligned} \right\} \quad (2)$$

In model tank tests, measurements were carried out at the midship position of the pusher–barge system; the longitudinal force X can be used as it is, but the lateral force Y and moment N need to be corrected for the distance from midship to the center of gravity of the pusher–barge system. The relationship of the midship lateral velocity v_m to the lateral velocity at the center of gravity of the pusher–barge system v is shown in Eq. 3 and the midship drift angle β_m is defined in Eq. 4:

$$v_m = v - x_G r' \quad (3)$$

$$\beta_m = \tan^{-1} \left(\frac{-v_m}{u} \right) \quad (4)$$

The hydrodynamic force that acts on the hull when a ship makes a diagonal turn is mainly caused by the dynamic pressure of the fluid. If the flow along the hull is to be related to the ship’s length, and the displacement of the hull is to be related to the draft of the ship, then the relationship of the flow and pressure can be related to the length overall (LOA) and the draft (d) as $LOA \times d$. Hydrodynamic forces (X_H, Y_H, N_H) on the ship’s hull based on the above consideration is shown in Eq. 5. In the equation, U is the ship’s speed ($U = \sqrt{u^2 + v^2}$):

$$\left. \begin{aligned} X_H &= (1/2)\rho LOA dU^2 X'_H(\beta_m, r') \\ Y_H &= (1/2)\rho LOA dU^2 Y'_H(\beta_m, r') \\ N_H &= (1/2)\rho LOA^2 dU^2 N'_H(\beta_m, r') \end{aligned} \right\} \quad (5)$$

where ρ is the water density, LOA is the length overall of pusher–barge system, d is the pusher–barge system’s draft, and r' is the nondimensional value of the yaw rate ($r' \equiv r LOA/U$). X'_H, Y'_H, N'_H are the hydrodynamic force coefficients defined as follows:

$$\left. \begin{aligned} X'_H &= X'_0 \cos^2 \beta_m + X'_{\beta\beta} \beta_m^2 + X'_{\beta r} \beta_m r' + X'_{rr} r'^2 \\ Y'_H &= Y'_\beta \beta_m + Y'_r r' + Y'_{\beta\beta\beta} \beta_m^3 + Y'_{\beta\beta r} \beta_m^2 r' \\ N'_H &= N'_\beta \beta_m + N'_r r' + N'_{\beta\beta\beta} \beta_m^3 + N'_{\beta\beta r} \beta_m^2 r' \end{aligned} \right\} \quad (6)$$

In the equation, X'_0 is the forward resistance coefficient of the pusher–barge system and $X'_{\beta\beta}, X'_{\beta r}, X'_{rr}, Y'_\beta, Y'_r, Y'_{\beta\beta\beta}, Y'_{\beta\beta r}, N'_\beta, N'_r, N'_{\beta\beta\beta},$ and $N'_{\beta\beta r}$ are the hydrodynamic derivatives for maneuvering. The hydrodynamic derivatives were obtained from model experiment data by using the least-squares method. $Y'_{\beta r}, Y'_{rr}, N'_{\beta r},$ and N'_{rr} were eliminated because in the circular motion tests, at

$r' = 0.2$, high accuracy for larger powers of r' was hard to achieve.⁵ The propellers of the pusher–barge system were located aft, and only contributed to the force in the x direction. The total force produced by the propellers as experienced by the pusher–barge system is defined as:

$$X_P = (1-t)\Sigma T \quad (7)$$

where t is the thrust deduction factor and ΣT is the total thrust produced by the propellers. T for each propeller is defined as:

$$T = \rho n_p^2 D_p^4 K_T(J_p, p) \quad (8)$$

where n_p is the propeller revolutions, D_p is the propeller diameter, K_T is the thrust coefficient, J_p is the propeller advance coefficient, and p is the propeller pitch ratio.

K_T for the propellers used in this study is assumed to have the characteristics shown in Eq. 9 and J_p is defined in Eq. 10:

$$K_T(J_p, p) = -0.3260 p J_p - 0.2005 J_p + 0.5234 p - 0.0398 \quad (9)$$

$$J_p = \frac{u(1-w_p)}{n_p D_p} \quad (10)$$

In Eq. 10, w_p is the propeller wake fraction, which changes with the drift angle β and also with the ship yaw rate r' . Hirano’s formula⁶ was used in calculating the wake fraction:

$$w_p = w_{p0} \exp[C_1 \beta_p^2] \quad (11)$$

where w_{p0} is the wake factor during the forward motion of the pusher–barge system, β_p is the drift angle at the propeller position ($\equiv \beta - \ell'_p r'$), and C_1 is the correction factor. ℓ'_p is the ratio of the distance from the propeller to the center of gravity of the pusher–barge system (with the forward direction having a positive value) to the length overall of the pusher–barge system. Rudder forces X_R and Y_R and moment N_R are defined as:

$$\left. \begin{aligned} X_R &= -(1-t_R)\Sigma F_N \sin \delta \\ Y_R &= -(1+a_H)\Sigma F_N \cos \delta \\ N_R &= -(x_R + a_H x_H)\Sigma F_N \cos \delta \end{aligned} \right\} \quad (12)$$

where δ is the rudder angle; $t_R, a_H,$ and x_H are the rudder and hull interaction parameters; and x_R is the x -

coordinate point on which the rudder force Y_R acts. The rudder normal force F_N is defined as:

$$F_N = \frac{1}{2} \rho A_R f_\alpha U_R^2 \sin \alpha_R \tag{13}$$

where A_R is the rudder area and f_α is the gradient of the lift coefficient of the rudder. f_α was estimated using Fujii’s formula.⁷ U_R is the flow velocity to the rudder and α_R is the effective rudder in-flow angle:

$$U_R = \sqrt{u_R^2 + v_R^2} \tag{14}$$

$$\alpha_R = \delta - \tan^{-1} \left(\frac{v_R}{u_R} \right) \tag{15}$$

where u_R is the water flow speed toward the rudder and v_R is the lateral flow speed after passing the propeller. v_R is calculated using Eq. 16; it is related to the rudder location and is influenced by the flow entrance angle to the rudder β_R ($\equiv \beta - \ell'_R r'$) and by γ_R , the flow rectification coefficient to the rudder. ℓ'_R is the ratio of the distance from the effective rudder position to the center of gravity of the pusher–barge system (with the forward direction being positive) to the length overall of the pusher–barge system:

$$v_R = U \gamma_R \beta_R \tag{16}$$

u_R is defined using Yoshimura’s formula:⁸

$$u_R = \frac{\epsilon u_p}{1-s} \sqrt{1 - 2(1-\eta\kappa)s + 1 - \eta\kappa(2-\kappa)s^2} \tag{17}$$

where s is the propeller slip ratio, η is the ratio of the propeller diameter to the rudder height, κ is the propeller flow correction factor ($\kappa = 0.6/\epsilon$ is normally used), and ϵ is the flow coefficient of the rudder with respect to its location.

4 Hydrodynamic force characteristics

4.1 Outline of the tank tests

The circular motion tests (CMTs) were carried out at the Hiroshima University Towing Tank (100 m × 7 m wide × 4 m deep). Each pusher–barge system without a propeller was tested at the corresponding full-scale speed of 7 knots and full-scale draft of 2.74 m. During the tests, the models were restrained from roll and heave motions but were free to trim. Force and moment transducers were placed at the midship position of the pusher–barge

system (at exactly half of the total length of the pusher and barge combination). The longitudinal force (X_H^*), lateral force (Y_H^*), and yawing moment (N_H) were measured and nondimensionalized using the following equations (the effects of virtual masses were added later to the measured longitudinal and lateral forces):

$$X_H^{*'}, Y_H^{*'} = \frac{X_H^*, Y_H^*}{(1/2)\rho LOA dU^2} \tag{18}$$

$$N_H' = \frac{N_H}{(1/2)\rho LOA^2 dU^2} \tag{19}$$

In the equation, asterisks denote results measured from experiments with the influence of virtual mass. There is no correction for N_H due to virtual mass, hence $N_H^* = N_H$.

4.2 Test results and hydrodynamic derivatives for maneuvering

Figure 5 shows the hydrodynamic force coefficient curves for the two-column arrangements (21BP, 22BP, 23BP) of the pusher–barge system as part of the CMT measured data⁵ of the longitudinal and lateral forces and yawing moment measured at the midship position of the pusher–barge systems (X_H^* , Y_H^* , N_H) in nondimensional form. In Fig. 5, the dashed lines shown are the fitted curves of the hydrodynamic derivatives based on Eq. 6 and show good accuracy.

Table 3 shows the hydrodynamic derivatives obtained from the model test data and the calculated added masses, moment of inertia, and course stability index, C . In Table 3, added mass coefficients (m'_x , m'_y , J'_{zz}) were calculated using the surface singularity distribution method, with the assumption of a rigid free surface for the ship. The added mass coefficients were nondimensionalized using the following expressions:

$$m'_x, m'_y = \frac{m_x, m_y}{(1/2)\rho LOA^2 d} \tag{20}$$

$$J'_{zz} = \frac{J_{zz}}{(1/2)\rho LOA^4 d} \tag{21}$$

The course stability index, C , is defined in Eq. 22. The rudder effect is not taken into account in the calculation of C . The negative values of the course stability index for configurations 11BP, 12BP, and 13BP show that these pusher–barge systems are unstable in course keeping; in contrast, 31BP has the largest positive value of course stability index, which means that it has the best performance in terms of course keeping.

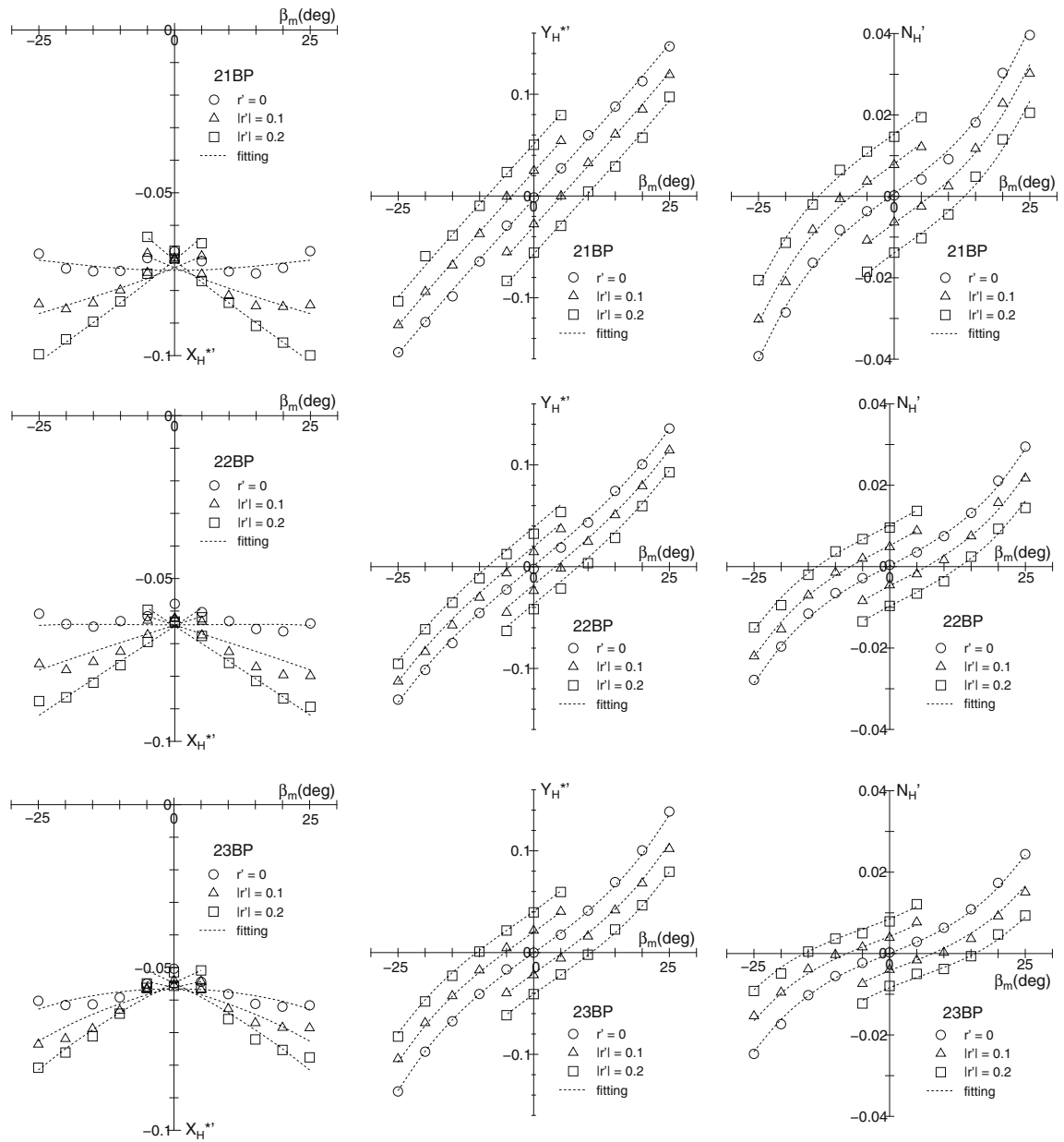


Fig. 5. Measured force and moment coefficients for configurations 21BP, 22BP, and 23BP. r' , the nondimensional the yaw rate; β_m , midship drift angle; X_H^{**} , non dimensional longitudinal-force; Y_H^{**} , non dimensional lateral-force; N_H' , non dimensional yawing moment

$$C = \frac{N'_r}{Y'_r - m' - m'_x} - \frac{N'_\beta}{Y'_\beta} \tag{22}$$

5 Effective power

The effective power requirement for a pusher–barge system was calculated based on the total resistance of the model tests at a ship speed of 7 knots; frictional resistance was calculated using the ITTC-1957 formula.

Figure 6 shows the effective power of the pusher–barge systems and Fig. 7 shows the effective power per unit barge for the various pusher–barge configurations. For pusher–barge systems that have the same number of barges, the required effective power can be summarized as 12BP < 21BP, 13BP < 31BP, and 23BP < 32BP. Pusher–barge systems that have a slender arrangement (smaller breadth but larger LOA) require less effective power to operate compared with wider and shorter arrangements.

Table 3. Resistance coefficient, hydrodynamic derivatives on maneuvering, added mass coefficients, and course stability index

Parameter	11BP	12BP	13BP	21BP	22BP	23BP	31BP	32BP	33BP
X'_0	-0.0428	-0.0355	-0.0322	-0.0738	-0.0642	-0.0566	-0.1	-0.0858	-0.0652
$X'_{\beta\beta}$	-0.0085	-0.0257	-0.0407	-0.0531	-0.0609	-0.0856	-0.0401	-0.0661	-0.1117
X'_{rr}	0.0376	0.0198	0.0435	0.0776	-0.0085	0.0446	0.0321	0.1128	0.0779
$X'_{\beta r} - m'_y$	-0.1197	-0.0659	-0.047	-0.1211	-0.113	-0.0789	-0.1442	-0.1004	-0.0022
Y'_β	0.2055	0.161	0.1586	0.3392	0.2544	0.219	0.3629	0.2442	0.2074
$Y'_r - m'_x$	-0.0006	-0.0003	-0.0415	0.0012	0.0122	-0.0477	-0.0206	0.0137	0.028
$Y'_{\beta\beta\beta}$	0.4912	0.7471	0.738	0.0498	0.2795	0.4809	0.1857	0.4957	0.6239
$Y'_{\beta\beta r}$	0.1146	-0.0367	-0.2819	-0.0443	-0.0777	-0.4078	0.1221	0.1332	-0.0947
N'_β	0.0627	0.057	0.0439	0.0553	0.0397	0.0308	0.0495	0.0517	0.0315
N'_r	-0.0406	-0.0288	-0.0323	-0.073	-0.0497	-0.0422	-0.1228	-0.0756	-0.0407
$N'_{\beta\beta\beta}$	0.0818	0.0803	0.0315	0.1995	0.1381	0.1291	0.1976	0.1137	0.0691
$N'_{\beta\beta r}$	-0.1497	-0.1763	-0.1205	-0.0903	-0.0789	-0.1791	-0.0566	-0.0989	-0.1106
m'_x	0.00706	0.00305	0.00176	0.00175	0.00076	0.00044	0.003	0.0013	0.00075
m'_y	0.00929	0.00667	0.00513	0.01017	0.00741	0.00574	0.01072	0.00787	0.00612
J'_{zz}	0.00048	0.0004	0.00033	0.00051	0.00043	0.00036	0.00054	0.00045	0.00038
C	-0.0416	-0.0856	-0.0145	0.1074	0.1079	0.0663	0.1635	0.0578	0.0491

The coefficients and derivatives are defined in Eqs. 6, 20–22

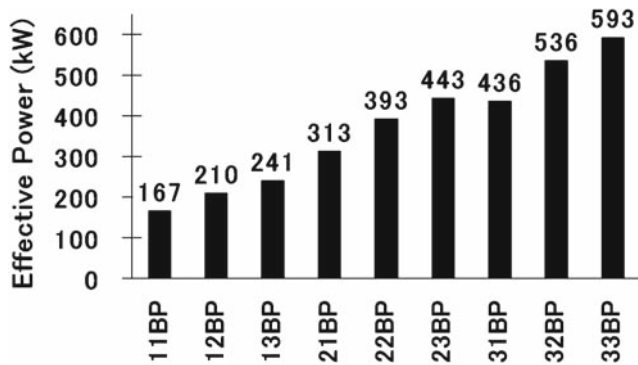


Fig. 6. Effective power comparison

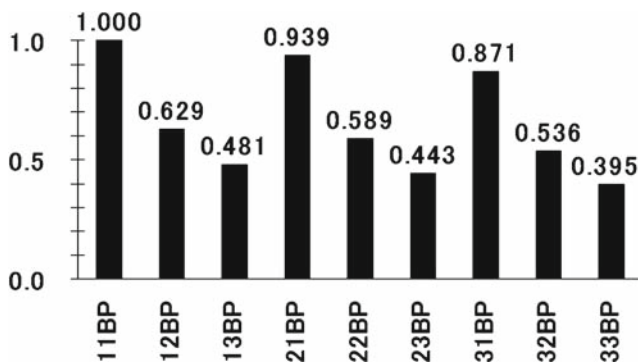


Fig. 7. Ratio of effective power per unit barge

6 Maneuverability

6.1 Outline of simulations

Maneuvering simulations of the pusher–barge systems were carried out using computer software written by

the authors in FORTRAN. The computer simulations include turning simulations at a 20° rudder angle, 10°/10° zigzag motion, and stopping simulation at a propeller pitch ratio of -0.8. Wind and waves were not taken into consideration in the simulations, and the water surface was assumed to be calm with the water of infinite depth and width (unbounded surface). Twin screws and twin rudders arranged symmetrically aft of the pusher were used. Controllable pitch propellers with a speed of 300 rpm were used in the simulations for maintaining a constant ship speed of 7 knots for the various pusher–barge configurations.

The hydrodynamic derivatives found in the previous section were used in the simulation program for maneuvering calculations. Other parameters used in the simulation program are shown in Table 4, with reference to data of a conventional twin-screw, twin-rudder vessel.⁹ These parameters were assumed to be the same for the nine different configurations.

Because the maneuvering of multiple barges is a relatively new field of study, verification and comparisons of the simulation results are restricted. Only the zigzag simulation was compared briefly (first overshoot angle) with experiments conducted at the Indonesian Hydrodynamic Laboratory (IHL),¹⁰ and it is advised that free-running model tests be conducted in the future for further verification of the simulation results.

6.2 Turning performance

Figure 8 shows the turning trajectories of the nine pusher–barge systems at a rudder angle of 20° and an initial forward speed of 7 knots. Figure 9 shows the tactical diameters, advances, and transfer distances of the

Table 4. Extra parameters used in computer simulations

Parameter	Symbol	Value
Thrust deduction fraction	t	0.164
Propeller wake fraction during initial forward speed	w_{p0}	0.34
Flow coefficient of rudder	ϵ	0.987
Rudder thrust deduction fraction	t_R	0.055
Rudder and hull interaction parameter	a_H	0.194
Flow rectification coefficient to the rudder	x'_H	-0.427
Ratio of effective rudder position to pusher-barge center of gravity	γ_R	0.23
	l'_R	-1.033

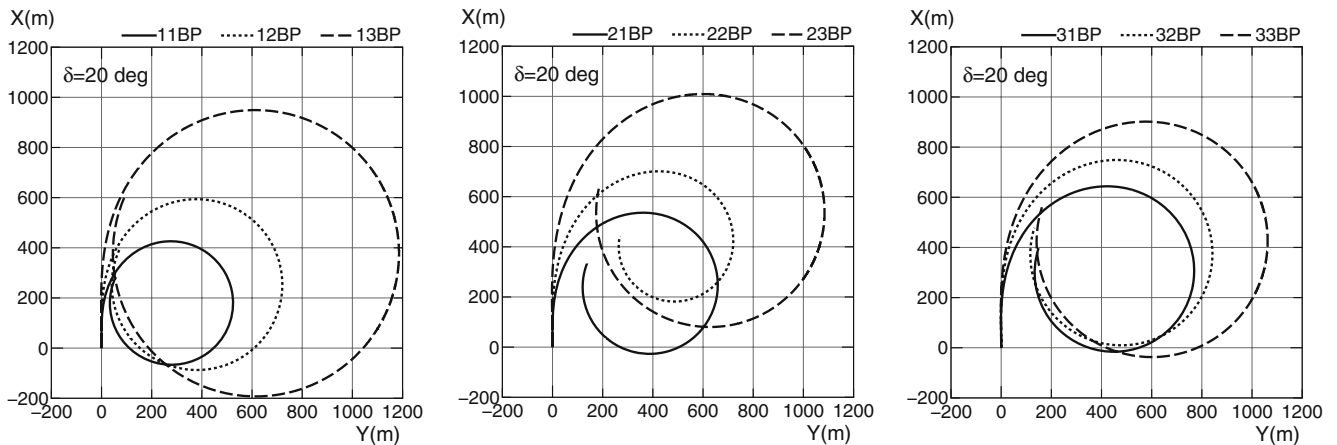


Fig. 8. Turning trajectories of pusher-barge systems (rudder angle $\delta = 20^\circ$)

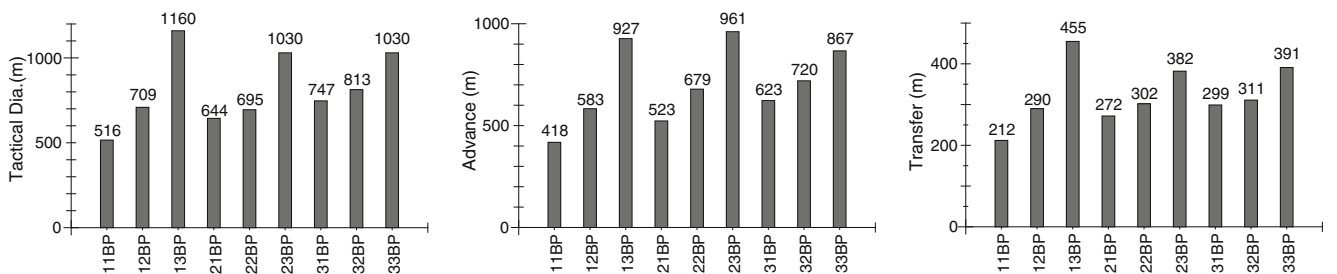


Fig. 9. Tactical diameters, advance distances, and transfer distances of pusher-barge systems ($\delta = 20^\circ$)

pusher-barge systems. When the number of barges is the same, the pusher-barge system with the larger LOA (barges arranged in a line, rather than in a row) requires a larger tactical diameter, advance, and transfer distance to turn compared to pusher-barge systems with a smaller LOA that are wider.

6.3 Zigzag performance

In the zigzag simulation, the rudder angle was set to change from 10° port to 10° starboard with a forward

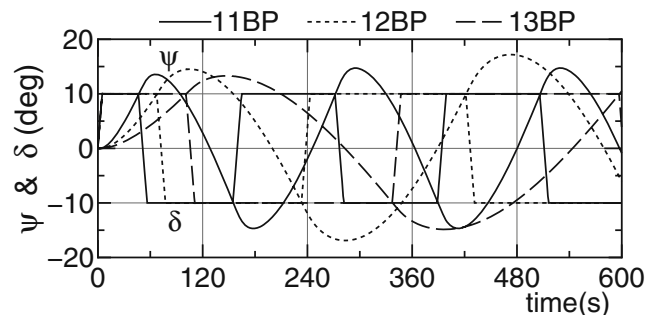


Fig. 10. Time histories of $10^\circ/10^\circ$ zigzag maneuvers for pusher-barge configurations 11BP, 12BP, and 13BP

Table 5. First and second overshoot angles

	First overshoot (degree)	Second overshoot (degree)
11BP	3.6	4.7
12BP	4.5	6.9
13BP	3.3	4.9
21BP	1.6	1.7
22BP	1.7	1.9
23BP	1.8	2.1
31BP	1.1	1.1
32BP	1.8	2.0
33BP	2.2	2.5

speed of 7 knots. Figure 10 shows the time histories of the zigzag maneuvers for pusher–barge configurations 11BP, 12BP, and 13BP, and Table 5 shows the first and second overshoot angles of the pusher–barge systems. From the table, overshoot angles of the pusher–barge systems are seen to be relatively small and all complied with IMO Criteria for Maneuvering, in which the first overshoot angle should not exceed 10° if LOA/U is less than 10 s (U = forward speed) and the second overshoot angle should not exceed the first overshoot angle by more than 15°. The first overshoot angles were compared with pusher–barge systems of the same configuration that were tested at the Indonesian Hydrodynamic Laboratory (IHL).¹⁰ The IHL data show first overshoot angles of 2.8°, 2.5°, 2.3°, and 1.9° for configurations 11BP, 12BP, 13BP, and 22BP, respectively. The tests were conducted in shallow water with a water height to draft ratio (h/d) of 2.0. Compared to the zigzag results in the current article, the first overshoot angles have a similar trend, except for configuration 12BP. The larger value of overshoot angle in the current article compared to the IHL data may be due to shallow water effects in the IHL tests. In our results, pusher–barge systems that have negative C values (11BP, 12BP, 13BP) also have the largest first overshoot angle, whereas the pusher–barge system that has the largest C value (31BP) has the smallest first overshoot angle.

The response times of the pusher–barge systems are shown in Fig. 11 and have the following relationships: 12BP > 21BP, 13BP > 31BP, and 23BP > 32BP. The response time was defined as the time between the first peak and the second peak in the zigzag graph (first period). When the number of barges is the same, pusher–barge systems with larger LOA arrangements (barges arranged in a line, rather than in a row) have a longer response time compared to pusher–barge systems with a smaller LOA but wider configuration. This is due to the significant increase in the moment of inertia when pusher–barge systems are arranged in a line.

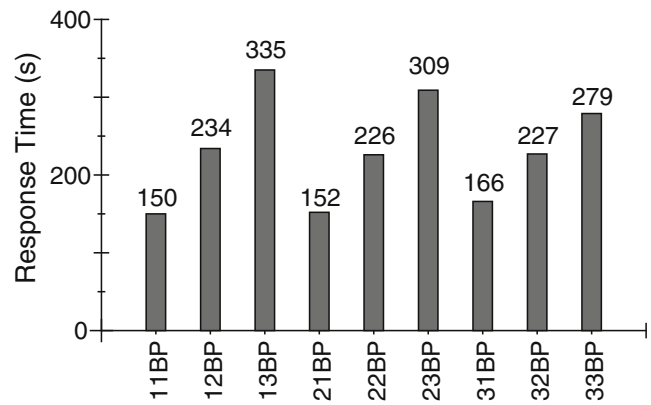


Fig. 11. Response times for 10°/10° zigzag maneuvers

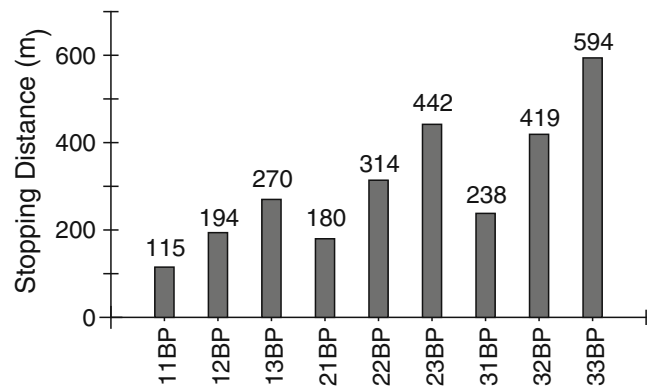


Fig. 12. Stopping distances with propeller reverse rotation at a propeller pitch ratio (p) of -0.8

6.4 Stopping performance

During stopping simulations, the rudder angle was set to zero at an initial forward speed of 7 knots. The speed was reduced by setting the propellers to a negative pitch ratio ($p = -0.8$). In the simulations, the propellers were assumed to undergo an instantaneous conversion from positive pitch ratio to negative pitch ratio. The time and distance required in real life for the propellers to reach the negative pitch ratio were not taken into account in the simulation. Stopping distances for the various pusher–barge systems are shown in Fig. 12, where 12BP > 21BP, 13BP > 31BP, and 23BP > 32BP. When the number of barges is the same, pusher–barge systems with larger LOA configurations (barges arranged in a line, rather than in a row) require more distance to stop than pusher–barge systems with a smaller LOA but a larger breadth. This is mainly due to the reduction of resistance when barges are arranged in a line (slender body), rather than in a row.

Table 6. Summary of pusher–barge system findings for the same number of barges arranged in a line or in a row

	Arranged in a line	Arranged in a row
Required effective power	Less	More
Tactical diameter	More	Less
Advance	More	Less
Transfer	More	Less
Response time	More	Less
Stopping distance	More	Less

7 Concluding remarks

Nine different configurations of pusher–barge system were studied. Captive model tests were conducted for each pusher–barge configuration and the hydrodynamic derivatives were found. In the comparison of effective power, it was found that at a service speed of 7 knots, pusher–barge systems with the same number of barges but arranged in a row (a smaller LOA but a larger breadth) required more power to operate compared to those with barges arranged in a line. In the maneuvering study, when the LOA increased, the tactical diameter, advance, and transfer distance required for turning motion increased as well. This was mainly due to the increased moment of inertia for pusher–barge systems when the LOA increases significantly. In the zigzag simulation, all pusher–barge systems had fairly small first and second overshoot angles and all complied with the IMO Criteria for Maneuvering. Pusher–barge systems with the same number of barges but arranged in a line (a smaller breadth but larger LOA) have a longer response time to the rudder angle of attack due to a significant increase in the moment of inertia when LOA increases. In the stopping simulation, pusher–barge systems with the same number of barges but arranged in a line (a smaller breadth but larger LOA) require a longer distance to stop due to the reduction in resistance for the slender body arrangement. The findings of this article are summarized in Table 6.

For future research and continued work, the following areas are to be considered: simulation accuracy, shallow water effects, the influence of restricted waterways, and unconventional arrangements of pusher–barge system.

Acknowledgment. The authors are grateful for the support given by a Grant-in-Aid for Scientific Research (No.17404022) from the Ministry of Education, Science and Culture of Japan.

References

1. Das PK, Varyani KS, Winkle IE, et al (2003) Assessment of load and strength of fastening systems on seagoing transportation barges. Workshop on Maritime Safety, Efficiency and Low Environmental Impact. 4–5 September 2003, Harbin, China
2. Grunthner GL (1962) Commercial transportation on the inland waterways. *Trans Soc Nav Archit Mar Eng* 70:84–127
3. Eda, H (1972) Course stability, turning performance, and connection force of barge systems in coastal seaways. *Trans Soc Nav Archit Mar Eng* 80:299–323
4. Pfennigstorf J (1970) *Handbuch der Werften X Band*. Bearb von K Wendel. Schiffahrts-Verlag HANSA, C Schroedter, Hamburg, p 11
5. Yasukawa H, Hirata N, Koh KK, et al (2007) Hydrodynamic force characteristics on maneuvering of pusher–barge systems (in Japanese). *J Jpn Soc Nav Archit Ocean Eng* 5: 133–142
6. Hirano M (1980) On the calculation method of ship maneuvering motion at the initial design phase (in Japanese). *J Soc Nav Archit Jpn* 147:144–153
7. Fujii H, Tuda T (1961) Experimental research on rudder performance (2) (in Japanese). *J Soc Nav Archit Jpn* 110: 31–42
8. Yoshimura Y, Nomoto K (1978) Modeling of maneuvering behavior of ships with the propeller idling, boosting and reversing (in Japanese). *J Soc Nav Archit Jpn* 144:57–69
9. Yoshimura Y, Sakurai H (1989) Mathematical model for the manoeuvring ship motion in shallow water (3rd report) (in Japanese). *J Kansai Soc Nav Archit Jpn* 211:115–126
10. Luhut TPS, Muis A, Muryadin (2005) Analysis study of train barge maneuvering in shallow water. Report of the 10th Seminar and Joint Meeting of the JSPS-DGHE Core University Program on Marine Transportation Engineering. Hiroshima University, Japan, 05-2:283–294